Acta Materialia 195 (2020) 698–707

Contents lists available at ScienceDirect

Acta Materialia

journal homepage: www.elsevier.com/locate/actamat

Full length article

Tailoring thermal properties of multi-component rare earth monosilicates

Mackenzie Ridley[a,*], John Gaskins[b], Patrick Hopkins[a,b], Elizabeth Opila[a,b]

[a] Department of Materials Science and Engineering, University of Virginia, Charlottesville, Virginia 22904, USA
[b] Department of Mechanical and Aerospace Engineering, University of Virginia, Charlottesville, Virginia 22904, USA

ARTICLE INFO

Article history:
Received 8 January 2020
Revised 3 June 2020
Accepted 8 June 2020
Available online 14 June 2020

Keywords:
Environmental barrier coating
Thermal expansion
Thermal conductivity
Rare earth silicates

ABSTRACT

This work explores the possibility of tailoring the thermal conductivity and thermal expansion of rare earth monosilicates through the introduction of multiple rare earth cations in solid solution. Six rare earth monosilicates are studied: Sc_2SiO_5, Y_2SiO_5, Nd_2SiO_5, Dy_2SiO_5, Er_2SiO_5, and Yb_2SiO_5. Four equimolar binary cation mixtures and a five-cation equimolar mixture were characterized. Thermal expansion was measured up to 1200 °C with X-Ray Diffraction (XRD) and bulk thermal conductivity was measured by Hot Disk technique. The linear coefficient of thermal expansion (CTE) of mixed-cation systems followed a rule of mixtures, with average linear CTEs between 6 - 9 × 10^{-6} /°C. Scandium monosilicate showed a lower linear CTE value as well as a notably lower degree of CTE anisotropy than other rare earth monosilicates. Thermal conductivity was found to decrease below rule of mixtures values through increasing heterogeneity in rare earth cation mass and ionic radii, as expected for the thermal conductivity of solid-solutions. The five-cation equimolar RE_2SiO_5 (RE=Sc, Y, Dy, Er, and Yb) shows a thermal conductivity of 1.06 W/mK at room temperature, demonstrating that multi-component rare earth silicates are strong candidates for novel dual-purpose thermal and environmental barrier coatings.

1. Introduction

1.1. Background

Ceramic matrix composites (CMCs) are considered effective alternatives for some nickel base superalloy components in hot sections of turbines. As of 2016, CMCs have even been introduced into commercial aircraft engines [1]. Silicon carbide (SiC) based CMCs (SiC/SiC) have a lower density and higher temperature capability than traditionally used superalloys, which allow for increased turbine efficiency through lowering engine weight and by increasing operating temperatures. When SiC is subjected to a combustion environment, it reacts with oxygen to form a silica scale, which concurrently undergoes a reaction with water vapor to form a volatile silicon hydroxide gas [2]. Volatilization of the oxide leads to recession of the CMC and eventual failure of the material. Environmental barrier coatings (EBCs) are needed as a protective layer to limit chemical interactions between the CMC and the environment. Thus, EBC candidates should be chemically stable with the combustion environment, SiC/SiC CMC, and silicon bond coat. Candidates should also have high melting temperatures, low CTE mismatch with the CMC, and good thermal shock resistance.

EBCs consist primarily of rare earth disilicates due to CTE match to both the silicon bond coat and CMC. Rare earth monosilicates exhibit superior chemical stability, lower thermal conductivity, limited number of polymorphs, and higher melting temperatures compared to their disilicate counterparts. Monosilicates are T/EBC candidates either within a monosilicate/disilicate mixture or as a top coat [3]. De-bonding and spallation from CTE mismatch and microcracking from elastic anisotropy currently prevent rare earth monosilicate usage as a single EBC layer for extended lifetimes.

Rare earth silicates also react with water vapor at high temperatures to form a volatile silicon hydroxide gas, although at lower rates than SiC. The respective reactions are shown in Eqs. (1) and (2) (RE=rare earth element).

$$RE_2Si_2O_7 + 2H_2O\ (g) \rightarrow RE_2SiO_5 + Si(OH)_4\ (g) \quad (1)$$

$$RE_2SiO_5 + 2H_2O\ (g) \rightarrow RE_2O_3 + Si(OH)_4\ (g) \quad (2)$$

The silica activity of $RE_2Si_2O_7$ + RE_2SiO_5 for yttrium and ytterbium rare earths are near 0.3 at 1600 K, while for RE_2SiO_5 + RE_2O_3 the activity of silica is closer to 0.003 [4,5]. The much lower silica activity of the RE_2SiO_5 + RE_2O_3 mixtures highlights the need to identify methods for tailoring rare earth monosilicates for use in

* Corresponding author.
E-mail address: mjr3be@virginia.edu (M. Ridley).

https://doi.org/10.1016/j.actamat.2020.06.012
1359-6454/

turbine applications. Computationally, Han et. al. hypothesize that rare earth cation mixing in monosilicates could lead to possible tailoring of water vapor resistance through adjustment of Si-O bond strengths [6]. It has also been shown with DFT and experimental work that flexural strength, elastic modulus, and thermal shock resistance are all dependent on rare earth cation mass for RE_2SiO_5 with the C2/c monoclinic crystal structure, termed the X2 structure [7]. Thermal expansion research has been mostly limited to mean expansion values via dilatometry, where no anisotropy is measured. Mixing of rare earth disilicates has been shown to produce a minimum in thermal conductivity at equimolar amounts through mass and bonding heterogeneity across the lattice [8], and is predicted to also occur for the monosilicate phase [3,9].

All RE_2SiO_5 are monoclinic and stable as either space group $P2_1/c$ or C2/c, which are generally termed the X1 and X2 structure, respectively [38]. X1 is the stable structure for larger rare earth cations La-Gd, while X2 is the stable structure for smaller cations Tb-Lu. For rare earth monosilicates showing both structures as polymorphs, X1 is stable at low temperatures while X2 appears at elevated temperatures. Each structure contains rigid silicon-oxygen tetrahedron and soft rare earth-oxygen polyhedron, where one oxygen atom position in each system is not a part of a Si-O tetrahedron and instead is loosely bound to rare earth atoms. Nd_2SiO_5 is the only X1 structure material discussed in this work. All other rare earth monosilicates (RE=Sc, Y, Dy, Er, or Yb) in this work appeared stable as the X2.

The goal of this research is to explore possibilities in tailoring thermal expansion and thermal conductivity of rare earth monosilicates by mixing rare earth cations. Results of binary equimolar mixtures of X2 monosilicates, $(RE,RE)_2SiO_5$ of (Dy,Er), (Dy,Sc), (Yb,Sc), and (Yb,Er), and a 5-cation equimolar mixture, RE_2SiO_5 (RE=Sc, Y, Dy, Er, and Yb), are explored alongside each single cation system. Multi-component rare earth cation systems are compared to their rule of mixtures values to elucidate how changes in average ionic radius and cation mass affect thermal expansion, CTE anisotropy, and thermal conductivity.

2. Experimental methods

2.1. Sample preparation

Mixed RE_2SiO_5 were made by blending equimolar ratios of pre-reacted single cation monosilicates (Praxair, United States). Starting Nd_2SiO_5 powder had an average diameter of 0.8 μm. All other initial powders were obtained as spray granules composed of 1 μm to sub-micron particles as shown in Fig. 1. Fine powders were desired to promote solid solution formation upon processing.

The purity of each starting powder was verified with a Panalytical Empyrean X-ray diffractometer (Malvern Panalytical, Westborough, MA). Starting powders and sintered products were characterized with X'Pert High Score Plus software to find unit cell parameters and phases present. In RE_2SiO_5 (RE=Y, Nd) no additional phases were detected by XRD or energy dispersive spectroscopy (EDS) techniques.

Powders were weighed to an accuracy of +/- 0.5 mg and mixed in equimolar ratios by dry ball milling for 24 h with stabilized zirconia ball mill media. Uniformly mixed powders were then loaded into a 20 mm diameter graphite die and consolidated by spark plasma sintering (SPS) using a Thermal Technologies DCS 25-10 SPS (Santa Rosa, CA). The SPS process was performed in argon, with a 10 to 20 minute hold at a maximum temperature and pressure of 1550-1700 °C and 65-70 MPa, respectively. After the SPS process, samples were annealed for 24 h at 1500 °C in air to remove residual carbon and restore oxygen stoichiometry.

Densities were calculated by ASTM standard (B962 – 15) Archimedes method with oil infiltration under vacuum to account for the impact of sample porosity on thermal conductivity measurements [10]. Single cation monosilicates showed densities of 92.5-98.8% relative density, binary solutions showed 90.2-96.2%, and the five-cation solution showed 86.8% relative density. For mixed rare earth cation monosilicates, crystal density was calculated via Rietveld refinement. Samples were polished to 1 μm using diamond suspension, then thermally treated at 1500 °C for 30 minutes in air to show grain boundary grooving. The microstructures were characterized with FEI Quanta LV200 Scanning Electron Microscope (SEM) with Energy Dispersive Spectroscopy (EDS). Transmission electron microscopy (TEM) was conducted with a Themis Z (Thermo Fisher Scientific: Waltham, MA). TEM sample preparation for the five-component RE_2SiO_5 included fine polishing with 0.05 μm colloidal silica.

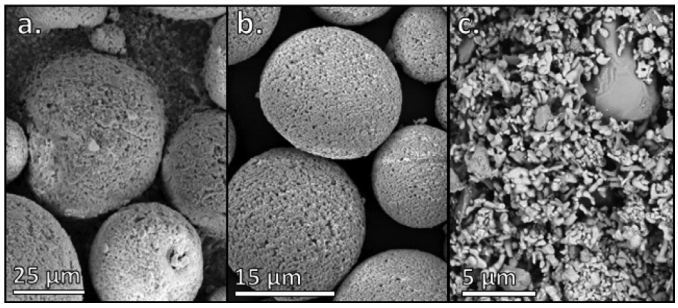

Fig. 1. a. Thermal spray powders of as-received Sc_2SiO_5, b. as-received Yb_2SiO_5, and c. $(Yb,Sc)_2SiO_5$ powder after ball milling for 24 h.

Coefficients of thermal expansion (CTE) were measured by hot stage XRD with an Anton Parr (Ashland, VA) HTK 1200N non-ambient stage. Measurements were made in air at 100 °C increments upon heating from room temperature up to 1200 °C with 60 °C/min heating rate. At each temperature increment, three XRD scans from 13-60° were acquired consecutively and combined by HighScore Plus software after measurement. Thermal conductivity was measured with Hot Disk, a transient plane source method where a sensor heats a sample through short current pulses and then measures thermal transport by time dependent resistivity changes [11–13]. Thermal transport is measured by fine control of electronic transport through the sensor, which is geometry dependent. Using this method, both thermal conductivity and thermal diffusivity are measured. The Hot Disk measurements were calibrated over a temperature range from room temperature up to 300°C by a SiO_2 reference sample, and agree well with literature values [14]. Room temperature values for each sample were measured along with temperature dependence for the five RE cation mixture RE_2SiO_5 (RE=Sc, Y, Dy, Er, and Yb) up to 300 °C.

3. Results

3.1. Phase stability

X-ray diffraction patterns of the single cation monosilicate components and the five rare earth cation monosilicate are shown in Fig. 2. Phase purity was characterized with the ICDD XRD patterns in HighScore Plus software. The Sc_2SiO_5 and Yb_2SiO_5 ICDD stick patterns are presented on the figure as a guide to the peaks associated with the monosilicate phases. Minor peaks corresponding to either a disilicate phase $RE_2Si_2O_7$ or a rare earth oxide phase RE_2O_3 are present from impurities in starting powder material. It can be seen that peaks for the five rare earth cation mixture are consolidated, representing a mixed rare earth silicate material.

Fig. 3 shows representative microstructures of single cation and mixed rare earth cation systems. EDS maps of each mixed cation sample (not included) show solid solution formation, with 1-10 μm

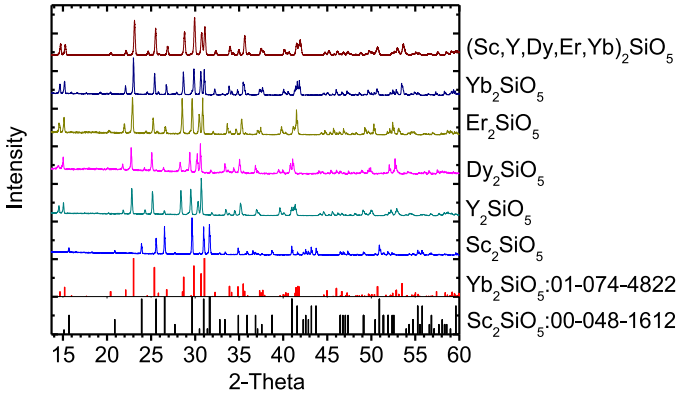

Fig. 2. X-ray diffraction of single cation monosilicates and a multi-component RE_2SiO_5, RE=Sc, Y, Dy, Er, and Yb.

clustering of single cations. The size of rare earth cation clustering corresponds to the size of rare earth oxide RE_2O_3 and/or disilicate $RE_2Si_2O_7$ impurities within the starting powders before and after ball milling. This implies that there is no phase separation of the RE_2SiO_5 mixed cation samples after the SPS processing and annealing procedure. As the number of rare earth element additions in each specimen increased, the bulk density was seen to decrease. It is possible that the decrease in density represents a resistance to sintering for multi-component rare earth silicates.

Energy dispersive spectroscopy (EDS) of the five-rare earth cation monosilicate system is shown in Fig. 4. Minor clustering of cation intensity on the maps correspond to starting impurities in the powders. Impurities suggested by the rare earth clustering in Fig. 4 were not noticeable in the XRD pattern.

Selected area electron diffraction (SAED) was also performed in order to resolve local segregation on the nanometer scale. Fig. 5 shows the SAED pattern of the [121] zone axis for the five-component RE_2SiO_5 as well as a simulated pattern of the [121] zone axis derived from XRD crystal data. A single monoclinic crystalline pattern is presented with no visible distortions or satellite peaks. TEM EDS is provided as supplementary information to this work.

3.2. Hot stage CTE

Unit cell dimensions for each sample were calculated from the X-ray data for each corresponding temperature. The differences in room temperature unit cell volume parameters were below 0.3% between measured and ICDD database values [15–18]. Results for the five-component RE_2SiO_5 are shown in Fig. 6 as a representative of the temperature dependent unit cell growth, where a, b, c, Beta angle, and unit cell volume are normalized to 1 for comparison. It can be seen that as the unit cell expands, X2 monosilicates show a decrease in the Beta angle as the unit cell moves towards a more orthorhombic type structure.

Table 1
Thermal expansion coefficients measured for Yb_2SiO_5 in powder and sintered form.

CTE x10^6/°C					
Yb_2SiO_5	a	b	c	Beta angle	Linear
Powder	2.65	6.59	10.5	−1.59	7.33
Sintered	2.73	6.57	10.3	−1.49	7.25

Table 2
Average linear CTE for single rare earth cation monosilicates from this study compared with literature values measured. *Refers to non-ambient XRD measurements.

RE_2SiO_5 RE Cation	Measured Linear CTE (XRD) 100–1200°C x10^6 /°C	Literature CTE x10^6 /°C	Literature Temperature Range (°C)
Sc	6.17	6.2 [21], 5-6 [22]	400-1400, 200-1400
Y	6.86	6.9 [23],*6.9 [24]	200-1350, 100-1200
Nd (X1)	8.91	9.9 [3]	400-1400
Dy	7.46	8 [21]	400-1400
Er	7.40	7.5 [25]	100-1300
Yb	7.25	7.2 [23],*6.3 [26]	200-1350, 200-1400

A comparison of average axial CTE from 100-1200 °C of Yb_2SiO_5 powder and sintered sample is shown in Table 1 in order to validate the provided X-ray diffraction data. Average axial CTE and volumetric CTE results between powder and sintered Yb_2SiO_5 samples agree well, which verifies that residual stresses do not significantly impact CTE results.

Unlike all X2 structure materials, X1 Nd_2SiO_5 stands out as the only material to show non-linear variation in unit cell parameters as temperature is increased up to 1200 °C, as seen in Fig. 7. Implications of this for CTE calculations of Nd_2SiO_5 are discussed later.

Linear CTE was calculated from the volume expansion divided by 3 to represent the average CTE in arbitrary directions x, y, and z, by the relationship $CTE = \frac{1}{3}\frac{\Delta V}{V\Delta T}$. These arbitrary directions do not necessarily correspond to a, b, and c axes due to the Beta angle being unequal to 90°. The CTE of the unit cell axes and Beta angle were calculated similarly, with the reference temperature being 20°C. Each a, b, and c direction and Beta angle for which axial CTE is calculated are defined in Fig. 8. The smaller blue atoms represent silicon, red atoms represent oxygen, and teal atoms represent a rare earth. Fig. 8b. shows Si-O tetrahedra displayed in blue, with only oxygen atoms that are not bonded within the Si-O tetrahedra shown in red. Rare earth cations and the oxygen unbonded to Si form directional chains alongside Si-O tetrahedra parallel to the c-axis direction.

Fig. 9 displays linear CTE for each single cation rare earth monosilicate from 100-1200 °C. The averages of the linear CTE for this temperature range are presented in Table 2 to compare with literature values. Literature comparisons of Yb_2SiO_5 and Y_2SiO_5 are

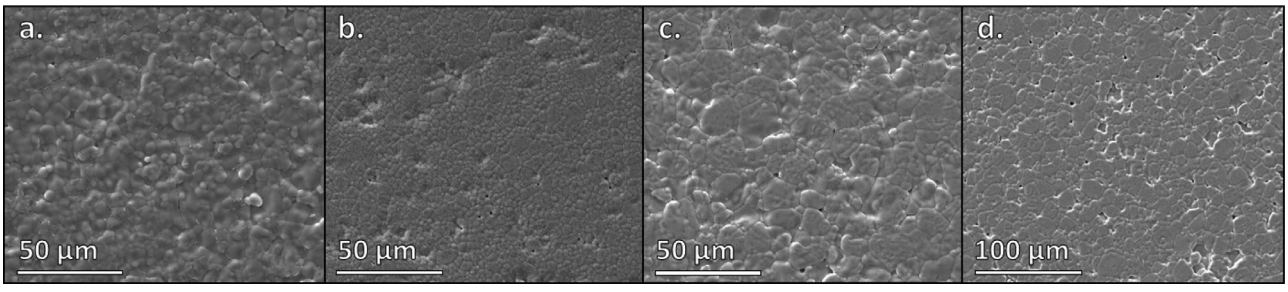

Fig. 3. Representative scanning electron micrographs of rare earth monosilicates after polishing and 1500°C anneal for 30 minutes to show grains. a. Y_2SiO_5, b. $(Dy,Er)_2SiO_5$, c. $(Yb,Sc)_2SiO_5$, d. Five-component RE_2SiO_5 (RE=Sc, Y, Dy, Er, Yb).

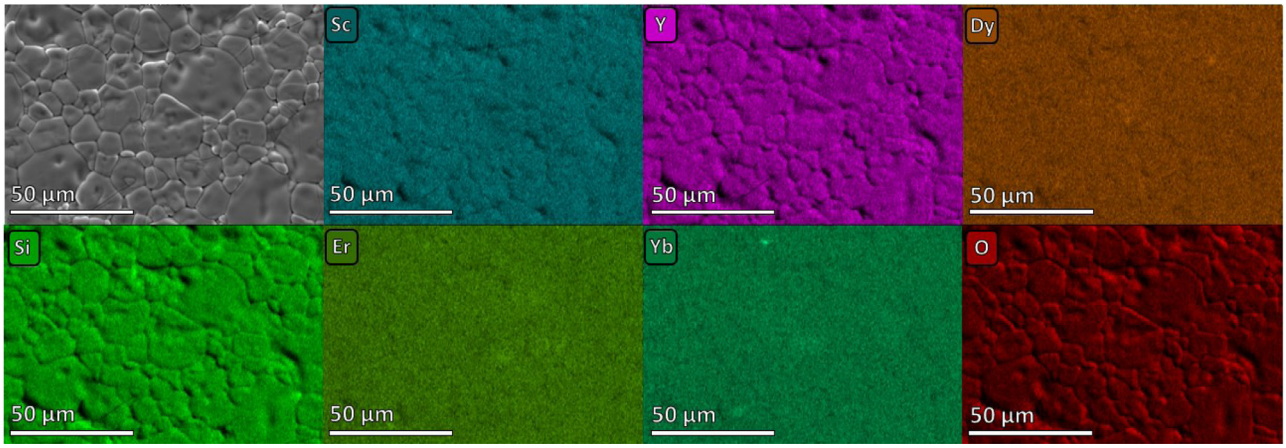

Fig. 4. Energy dispersive spectroscopy maps for the five-component RE_2SiO_5 (RE=Sc, Y, Dy, Er, Yb).

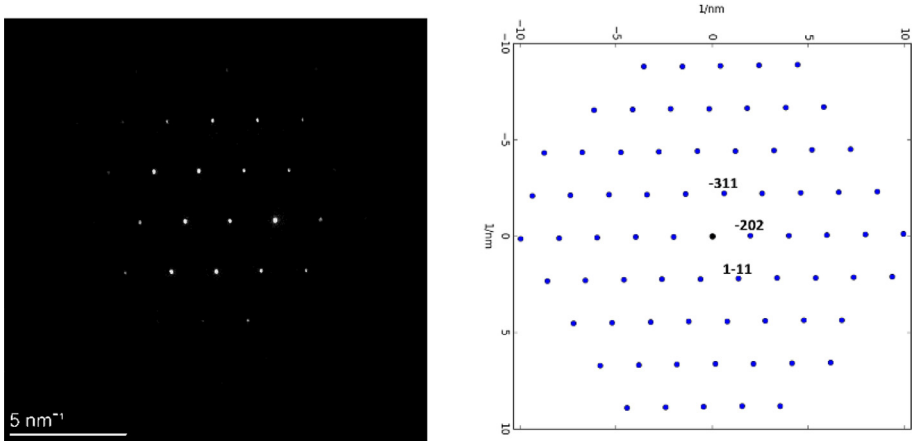

Fig. 5. Selected area electron diffraction showing the [121] zone axis of the five-component RE_2SiO_5 (RE=Sc, Y, Dy, Er, Yb) and a simulated hkl plot with parameters derived from XRD refinement.

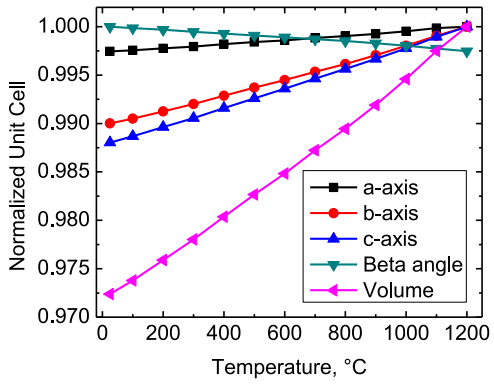

Fig. 6. Five-component RE_2SiO_5 (RE=Sc, Y, Dy, Er, Yb) normalized unit cell parameters from hot stage XRD refinements.

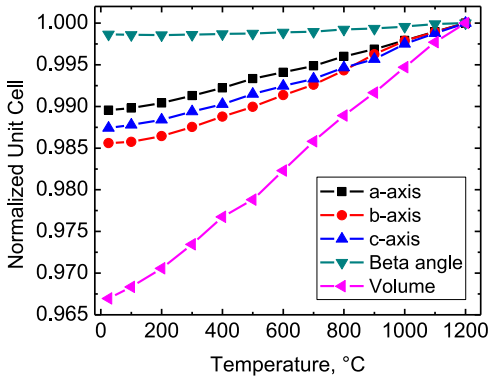

Fig. 7. X1 structure Nd_2SiO_5 unit cell expansion from hot stage XRD refinements.

also from hot stage XRD, while all other comparisons come from dilatometric techniques. X1 monosilicate Nd_2SiO_5 shows a higher linear CTE than all X2 RE_2SiO_5 in this study. Sc_2SiO_5 shows the lowest linear CTE, and has the closest CTE match to SiC [19], a silicon bond coat [20], and to low CTE rare earth disilicates EBC candidates [17].

Fig. 10 shows the directional axis CTE values for all single cation rare earth monosilicates. Initially it can be seen that X1 Nd_2SiO_5 shows unique CTE behavior for each direction of its unit cell. The thermal expansion of the Nd_2SiO_5 is highly temperature dependent up to 1000°C, especially in the b-axis. X2 monosilicates (Sc, Y, Dy, Er, and Yb) show a low a-axis CTE below 3.64×10^{-6} /°C. C-axis CTEs are close to an order of magnitude greater than the a-axis CTEs, with values of 9-10 $\times 10^{-6}$ /°C. Sc_2SiO_5 shows the lowest linear CTE and least amount of CTE anisotropy of the X2 structure monosilicates. The axis CTE results from single cation monosilicates were used to determine if mixed rare earth cation monosilicates show an average CTE value, or if linear CTE could be tailored beyond a rule of mixtures. Specifically, Sc_2SiO_5 additions were evaluated as a means to lower the overall degree of anisotropy.

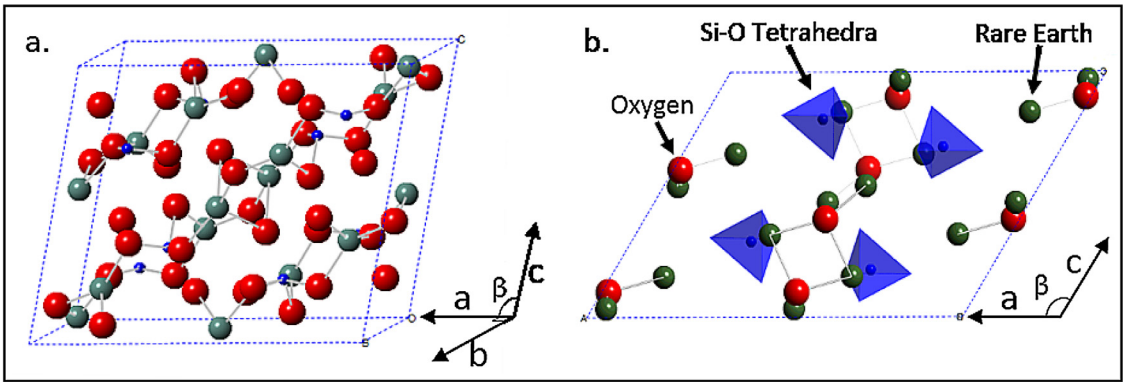

Fig. 8. X2 structure RE_2SiO_5 unit cell a. perspective and b. viewed from the b-axis. Only oxygen atoms that are not bonded to the Si-O tetrahedra are shown.

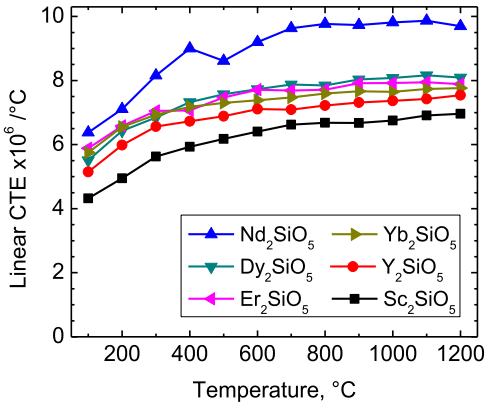

Fig. 9. Linear CTE of single cation RE_2SiO_5 from 100°C to 1200 °C.

$(RE,RE)_2SiO_5$ of (Dy,Er), (Dy,Sc), (Yb,Sc), and (Yb,Er) axis CTEs are displayed against their rule of mixtures (ROM) average in Fig. 11. Each axis CTE is labelled on the graph and is associated with both colored and grey data points. The colored data points represent measured CTE values for the given axis. Solid gray data points represent ROM determined from single rare earth cation measurements, shown previously in Fig. 10. Measured linear CTE and the rule of mixtures linear CTE are shown as lines in color and in gray, respectively. (Yb,Er) and (Dy,Er) mixtures represent combinations of two rare earth cations of similar mass and ionic radii, while (Yb,Sc) and (Dy,Sc) show results of more widely varying mass and ionic radii. CTE results within 0.5×10^{-6}/°C are considered insignificant differences for comparison of results. All systems show linear CTE that are close to ROM, while larger deviations are present in terms of CTE anisotropy. The (Dy,Er) and (Yb,Er) mixtures both show slightly lower values than predicted ROM but differences are within 0.5×10^{-6}/°C.

Fig. 12 shows the axis CTEs for the five-component RE_2SiO_5 in comparison with the predicted rule of mixtures values. From the graph, it is seen that linear CTE (solid line) does generally follow a ROM. Still, the c-axis CTE, as well as the Beta angle CTE not shown here, show larger differences. This c-axis deviation from ROM shows that scandium additions do not decrease CTE anisotropy for the five-component mixture as predicted by ROM, even while the linear CTE remains in bounds of a ROM prediction.

3.3. Hot disk measurements of thermal conductivity

The Hot Disk technique allows for direct measurement of diffusivity (D) and thermal conductivity (κ) with specific heat (C_P) being approximated by Neumann-Kopp rule from the constituent oxides. The relationship is shown in Eq. (3) where ρ represents the theoretical compound density. Values are corrected for effect of porosity and cracking by the Maxwell-Gernett model [27] Eq. (4) where ϕ represents the relative porosity percentage of each sample.

$$\kappa = DC_P\rho \tag{3}$$

$$\kappa_{Solid} = \frac{\kappa_{Porous}}{\left(\frac{1-\phi}{1+\phi}\right)} \tag{4}$$

A summary of measured thermal conductivity values, as well as values corrected for porosity are shown tabulated in Table 3 and graphically in Fig. 13. An uncertainty of 3% was assigned to the density measurements, which was incorporated into the hot disk measurement uncertainty. Values presented in Table 3 are still impacted by other bulk features such as impurity phases or grain boundaries.

Y_2SiO_5 thermal conductivity was experimentally measured by Sun et al. who reported a value of 1.86 W/mK at room temperature [28], which is similar to the value measured in this study. Literature values of measured room temperature thermal conductivity values are as follows: Dy_2SiO_5 ~ 1.9 W/mK, Yb_2SiO_5 ~ 2.2 W/mK, Er_2SiO_5 ~ 2.7 W/mK, and Y_2SiO_5 ~ 3.5 W/mK [7]. The samples reported on in this work have slightly lower thermal conductivities, which could be due to microstructural differences such as grain size variations. The ranking of thermal conductivity values in this study remains comparable to both experimental and computational results by Tian et al [7]. Ranking from lowest to highest thermal conductivity: Dy_2SiO_5, Yb_2SiO_5, Er_2SiO_5, and Y_2SiO_5. Additionally, a measured thermal conductivity for hot pressed Nd_2SiO_5 of ~ 2.8 W/mK at room temperature was reported in the literature [21], which is comparable to the value of 2.31 ± 0.18 W/mK presented in this study. The five-component rare earth silicate shows a low room temperature thermal conductivity of 1.06 ± 0.04 W/mK. In addition to possessing a thermal conductivity lower than each of the individual or binary cation monosilicates, the five-component RE_2SiO_5 (RE=Sc, Y, Dy, Er, Yb) shows a relatively flat trend over the temperature range tested in this study. While thermal conductivity was not tested up to relevant operating temperatures for EBC materials, previous literature has shown that the thermal conductivity of RE monosilicates is relatively flat above 300°C [29,30]. This suggests that the thermal conductivity of ~ 0.9 W/m/K at 300°C serves as a conservative upper bound for the thermal conductivity at elevated temperatures. A similar reduction in thermal conductivity at room temperature, compared to the constituent materials, of high entropy ceramics has recently been shown for similar multi-cation high entropy borides and silicides, and entropy stabilized oxides [31–33].

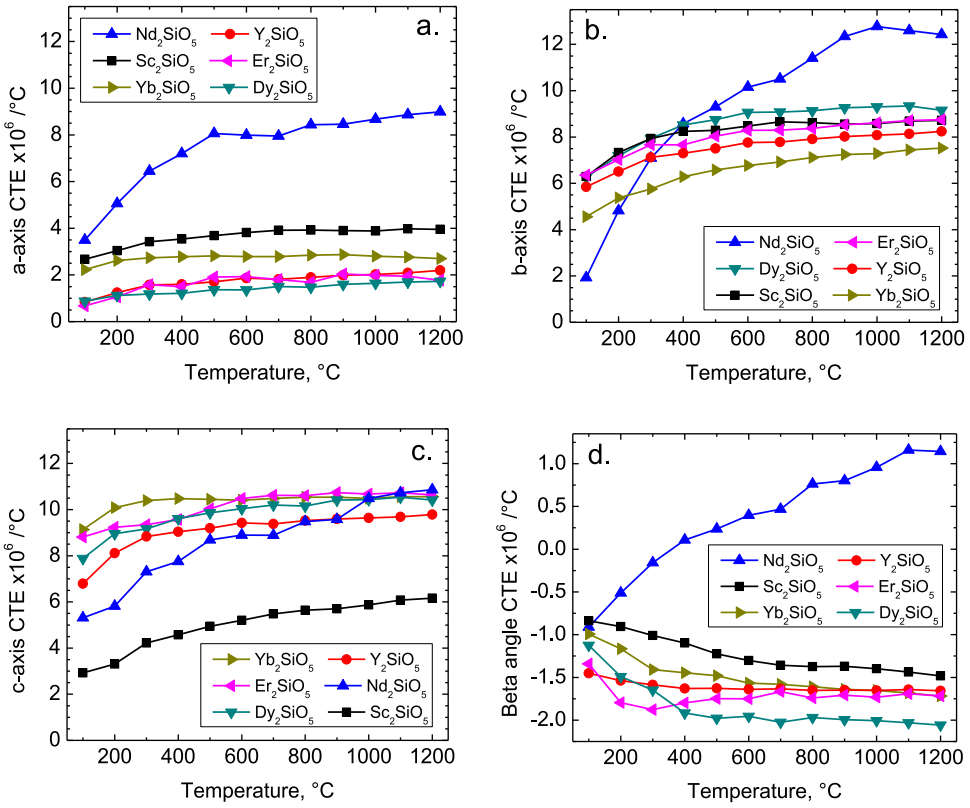

Fig. 10. Axial CTEs for each single cation RE_2SiO_5. a. a-axis, b. b-axis, c. c-axis, and d. Beta angle.

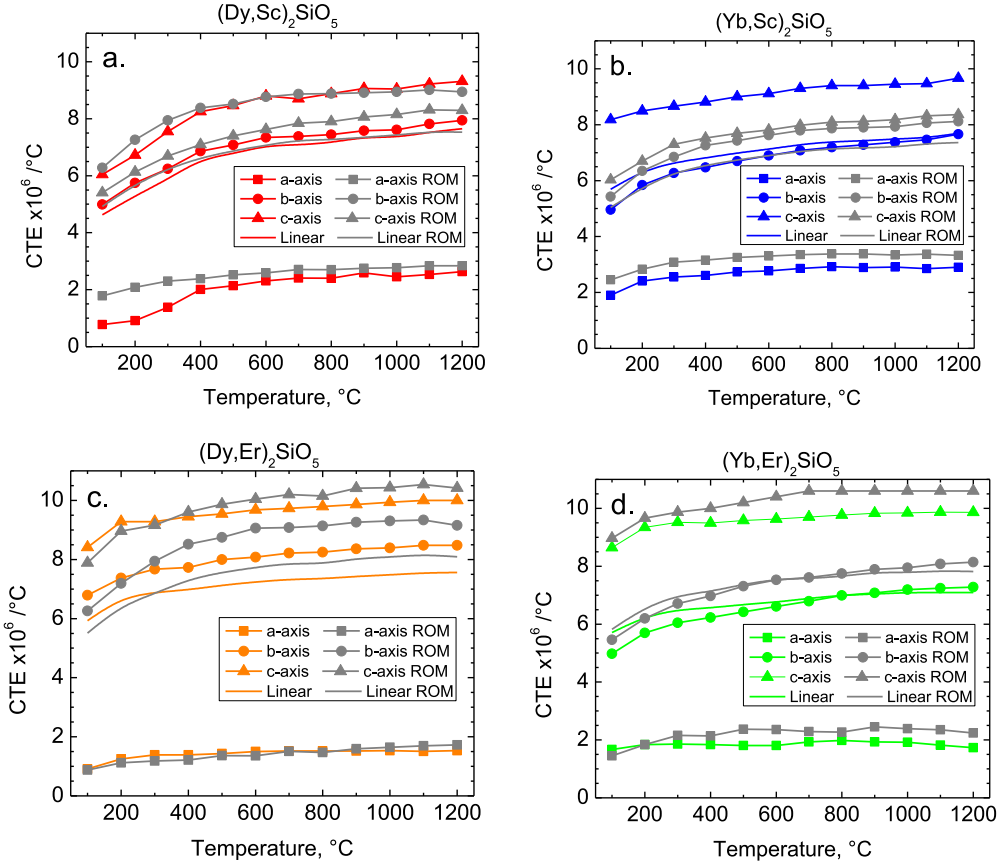

Fig. 11. Axial and linear CTE values for binary equimolar mixtures $(RE,RE)_2SiO_5$ compared to ROM values calculated from constituent RE_2SiO_5: a. $(Dy,Sc)_2SiO_5$, b. $(Yb,Sc)_2SiO_5$, c. $(Dy,Er)_2SiO_5$ and d. $(Yb,Er)_2SiO_5$.

Table 3
Room temperature thermal conductivity measured values for RE_2SiO_5 and values corrected for density.

Rare Earth Cations	Measured W(m K)$^{-1}$	Density Corrected W(m K)$^{-1}$	Five cation RE_2SiO_5 Temperature °C	Measured W(m K)$^{-1}$	Density Corrected W(m K)$^{-1}$
Sc	2.41 ± 0.05	2.80 ± 0.10	20	0.93 ± 0.02	1.06 ± 0.04
Y	1.95 ± 0.05	2.08 ± 0.08	50	0.90 ± 0.04	1.02 ± 0.06
Nd	2.26 ± 0.16	2.31 ± 0.18	100	0.88 ± 0.04	1.00 ± 0.05
Dy	1.02 ± 0.02	1.15 ± 0.04	150	0.87 ± 0.03	0.98 ± 0.05
Er	1.30 ± 0.03	1.47 ± 0.06	200	0.85 ± 0.03	0.96 ± 0.04
Yb	1.23 ± 0.04	1.36 ± 0.06	250	0.84 ± 0.03	0.95 ± 0.04
(Yb,Y)	1.24 ± 0.05	1.37 ± 0.07	300	0.76 ± 0.03	0.86 ± 0.04
(Dy,Sc)	1.01 ± 0.03	1.09 ± 0.05			
(Dy,Er)	1.24 ± 0.19	1.34 ± 0.21			
(Yb,Er)	1.08 ± 0.03	1.32 ± 0.05			

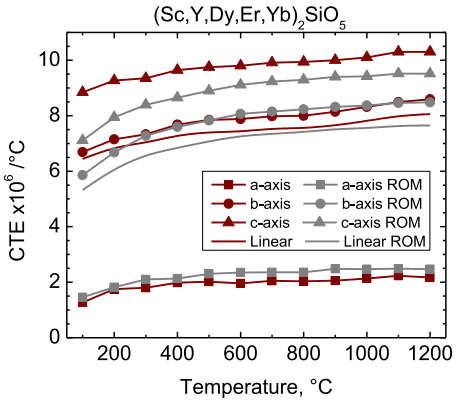

Fig. 12. Axial and Linear CTE values for five-component RE_2SiO_5, (RE=Sc, Y, Dy, Er, Yb) compared to ROM values.

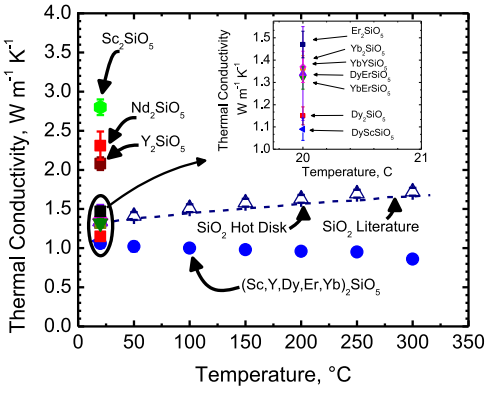

Fig. 13. Room temperature thermal conductivity values of RE_2SiO_5 measured by Hot Disk method, with values corrected for apparent density. The five-component RE_2SiO_5 (RE=Sc, Y, Dy, Er, Yb) and SiO_2 are measured up to 300°C.

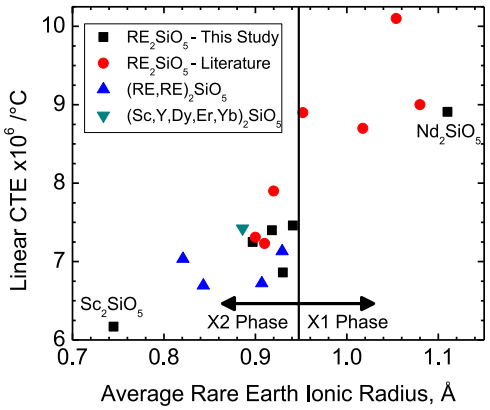

Fig. 14. Linear CTE comparison to ionic radii, including all systems in this study along with other literature single cation RE_2SiO_5, where RE= Y(X1), Sm, Gd, Tb, Ho, Tm, and Lu.

4. Discussion

4.1. CTE

Fig. 7 shows a unique thermal expansion feature of Nd_2SiO_5, the representative X1 structure in this study. While both X1 and X2 monosilicates show a decreasing Beta angle at low temperatures, the X1 structure Beta angle starts increasing near 300 °C. This produces non-linear results in both linear and axial CTE. It is uncertain if this trend holds true for other RE_2SiO_5 with the X1 structure.

Linear CTE for each sample can be compared to average ionic radii for the two rare earth cation sites within the unit cell, as shown in Fig. 14. Single cation monosilicates from this study and from literature are presented alongside equimolar rare earth cation mixtures, displaying a positive correlation between ionic radii and linear CTE. Points on this graph with ionic radii above 0.95 Å are X1, while all points below are X2 structure monosilicates. Other rare earth cations in RE_2SiO_5 from literature are as follows: Y(X1 structure) [24], Sm [34], Gd [35], Tb [7], Ho [36], Tm [7], and Lu [35].

The standard deviation of rare earth cation mass was calculated for each sample to represent the spread of rare earth cation mass for each material relative to an average rare earth cation mass. This method for comparison was chosen to display how mixing of rare earth cations with similar mass (small standard deviation) could produce differing thermal properties than from mixing rare earth cations with widely varying mass (large standard deviation). Fig. 15a shows that there is negligible effect of cation mass differences in mixed cation rare earth monosilicates on linear CTE. X2 structure single cation and multi-rare earth cation monosilicates show linear CTE values between 6 and 7.5 × 10^{-6} /°C. Ren et al. state that a multi-component RE_2SiO_5 (RE=Y, Ho, Er, and Yb) showed CTE that deviated from a ROM [30], which is contradictory to the results of this work. It was hypothesized in their work that increased lattice distortion from the multiple components led to an increase in elastic stiffness. Therefore, CTE decreased by -11.3% and Young's Modulus was increased 7.4% relative to the ROM values. Dong et al. report the CTE of an equiatomic 5 cation $RE_2Si_2O_7$ (RE=Sc, Y, Gd, Yb, Lu) to be between 3.7 and 5.7 × 10^{-6} /°C in the temperature range of 300°C to 1350°C [37]. While the ROM value is not discussed by the authors, a ROM value can be estimated from data provided by Turcer et. al. in their Fig. 3, which displayed the average CTE of the rare earth disilicates [3]. The ROM value for the five cation $RE_2Si_2O_7$ (RE=Sc, Y, Gd, Yb, Lu) is around 4.9 × 10^{-6} /°C, which agrees well with the result presented in this work that the CTE of multiple cation rare earth silicates can be approximated by a ROM value.

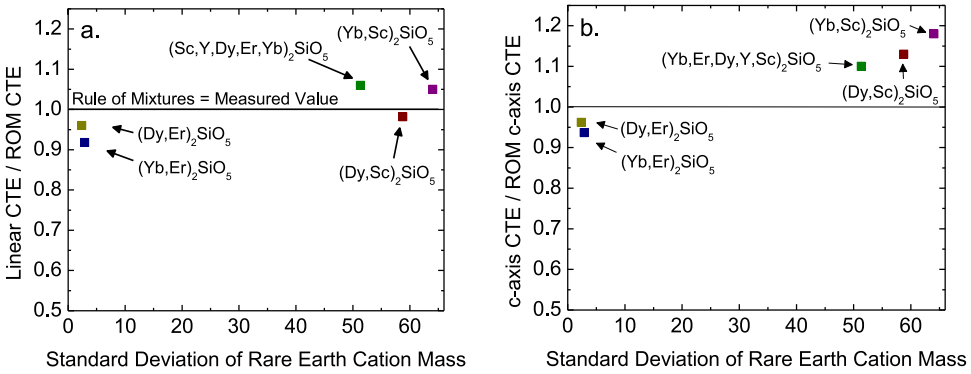

Fig. 15. a. Linear CTE ratio and b. C-axis CTE ratio, compared to the standard deviation of rare earth cation mass for RE_2SiO_5 mixtures.

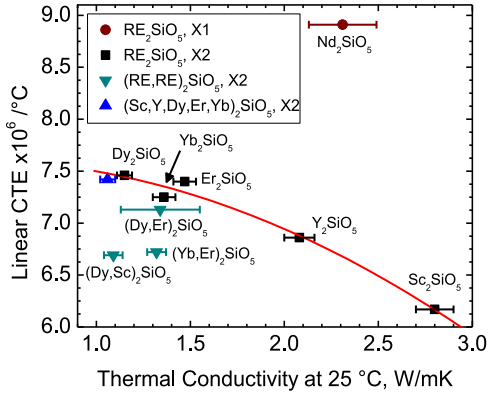

Fig. 16. Room temperature thermal conductivity measurements compared to average linear CTE (100°C–1200°C).

Differences in anisotropy between mixed and single rare earth cation monosilicates are also minimal. Fig. 15b displays the minor trend of c-axis CTE ratio to the ROM value, where the c-axis CTE increases with increasing cation mass standard deviation. This shows that additions of lightweight scandium cation in solution does not decrease anisotropy as predicted by the rule of mixtures. It is hypothesized that the scandium, the smallest cation in this study, interacts less with the rigid Si-O tetrahedron in the structure.

Felsch characterized the rare earth silicates as containing strong covalently bonded Si-O tetrahedron and comparatively soft ionically bonded RE-O polyhedra [38]. Further, the Si-O bonding in many silicates has been shown to have near zero thermal expansion, which points to the thermal expansion being governed by rare earth oxygen bonds [39]. Viewing the X2 unit cell along the b-axis helps to explain the anisotropy of X2 monosilicates, as shown in Fig. 8b. The c-axis shows the greatest CTE because this direction has planes where no Si-O tetrahedra inhibit expansion of the rare earth polyhedra. Similarly, the a-axis direction has the highest density of rigid Si-O tetrahedron, which explains the low a-axis CTE of $1 - 3 \times 10^{-6}$ /°C. Nd_2SiO_5, being X1 structure monosilicate with different bonding characteristics, displayed higher CTE values but overall, decreased CTE anisotropy.

4.2. Thermal conductivity

An inverse correlation between linear CTE and thermal conductivity for single rare earth cation X2 monosilicates is seen in Fig. 16, where the fit line is used to guide the eye. For example, Dy_2SiO_5 has the largest linear CTE of the single cation monosilicates measured, and also shows the lowest thermal conductivity at room temperature. The X1 Nd_2SiO_5 does not fit the trend due to significantly different expansion trends. Mixed cation X2 systems have lower thermal conductivities, presumably due to increased phonon scattering with mixed mass and ionic sizes.

A general trend with multi-component RE_2SiO_5 systems is that mixing decreases thermal conductivity more with each additional cation added in mixing. $(Dy,Er)_2SiO_5$ appears as the only exception in this study, which could arise from differences in bulk defects such as grain size or alternate phases. Fig. 17 shows the ratio of measured and ROM thermal conductivity values plotted against the standard deviation of the rare earth cation mass and the ionic radius for each mixture. These results demonstrate that thermal conductivity can be most effectively tailored below the ROM value through further increasing the lattice heterogeneity. This trend has been validated in previous studies where deviations from a ROM thermal conductivity are attributed to phonon scattering from increased lattice disorder, where disorder stems in this case from rare earth cation mass and bonding heterogeneity [7–9].

Further studies looking at three and four component mixtures may shed more light on the structure-property relationships between the rare earth cations and relevant thermal properties for EBCs. Using the observations for the various binary systems as well as the five-component system, future rare earth compositions could be tailored to further decrease thermal conductivity by increasing heterogeneity in the crystal lattice. Additionally, the high temperature thermal conductivity of multi-component rare earth silicates should be addressed for optimized mixtures that may represent novel EBC material candidates.

5. Conclusions

The degree of CTE anisotropy in X2 structure rare earth monosilicates was quantified by high temperature XRD. The results show that scandium monosilicate has a significantly lower degree of CTE anisotropy than other X2 materials. Mixed rare earth cation monosilicates followed a rule of mixtures for tailoring CTE, while a weak dependence of c-axis CTE anisotropy on cation mass is seen. The high and anisotropic CTEs are not appropriate for a single layer EBC material on SiC-based CMCs. Both the high linear CTE and significant CTE anisotropy should be taken into account when considering rare earth monosilicates for designing rare earth silicate EBCs.

Thermal conductivity of mixed rare earth cation monosilicates follows a rule of mixtures when rare earth cations of similar ionic radii and mass were combined. Thermal conductivity can be reduced by increasing heterogeneity in both cation mass and ionic radii. The $(Dy,Sc)_2SiO_5$ mixture contained the largest difference in

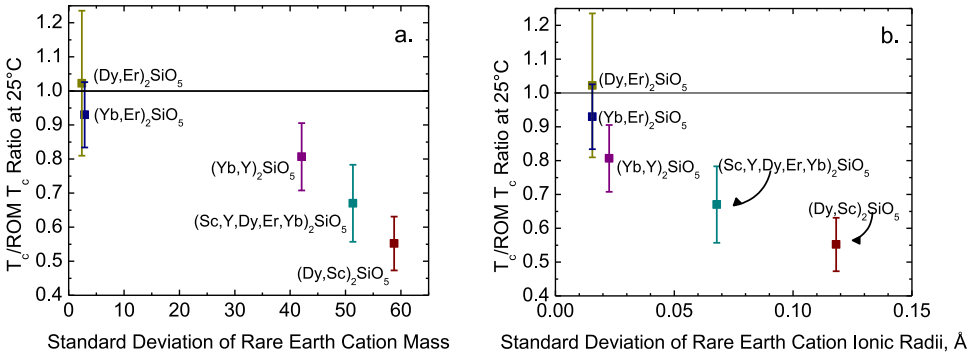

Fig. 17. Ratio of thermal conductivity to its ROM value plotted against the a. standard deviation of rare earth cation mass and b. standard deviation of rare earth ionic radius for each RE_2SiO_5 mixture.

rare earth cations mass for the RE lattice sites and also showed the greatest decrease in room temperature thermal conductivity from a ROM. A five-component RE_2SiO_5 provided the lowest thermal conductivity value, with a room temperature value of 1.06 W/mK that further decreases upon heating to 300°C. The five-component rare earth monosilicate also showed a relatively high linear CTE of 7.42×10^{-6} /°C which agrees with an inverse correlation between CTE and thermal conductivity observed for single cation X2 structure rare earth monosilicates. The ability to lower thermal conductivity to near 1 W/mK at room temperature has been shown for mixed rare earth cation monosilicates, and allows for potential to tailor thermal properties of EBC systems for future increases in turbine operating temperatures.

Declaration of Competing Interest

The authors declare that they have no known competing financial interests or personal relationships that could have appeared to influence the work reported in this paper.

Acknowledgements

This work was supported by program manager Adam Chamberlain and Rolls-Royce Inc. task order # 17-UVA-26, “Entropy Stabilized Silicate Investigation,” PI Elizabeth Opila, task order # 18-UVA-26, “Characterization of Thermal Properties and Chemical Stability of High Entropy Rare Earth Monosilicates,” co-PIs Patrick Hopkins/Elizabeth Opila, and the University of Virginia SEAS 2017-2018 Research Innovation Award, “Center for Exploring and Tailoring Thermal Conductivity of Defective Oxides” PI Elizabeth Opila, co-PIs Keivan Esfarjani, Patrick Hopkins, Jon Ihlefeld, Haydn Wadley. This work was partially supported by the National Science Foundation, Grant Number CBET-1706388. Thanks to Dr. Bryan Harder (NASA Glenn Research Center) for supplying RE_2SiO_5 powders and Dr. Helge Heinrich (University of Virginia) for TEM.

Supplementary materials

Supplementary material associated with this article can be found, in the online version, at doi:10.1016/j.actamat.2020.06.012.

References

[1] G. Gardiner, Aeroengine Composites, Part 1: The CMC invasion, Composites World, 2015.
[2] E.J. Opila, J.L. Smialek, R.C. Robinson, D.S. Fox, N.S. Jacobson, SiC recession caused by SiO_2 scale volatility under combustion conditions: II, thermodynamics and gaseous-diffusion model, J. Am. Ceramic Soc. 82 (7) (1999) 1826–1834.
[3] L. Turcer, Towards multifunctional thermal environmental barrier coatings (TEBCs) based on rare-earth pyrosilicate solid-solution ceramics | Elsevier Enhanced Reader, Scripta Materialia (154) (2018) 111–117.
[4] N. Jacobson, Silica activity measurements in the Y_2O_3-SiO_2 system and applications to modeling of coating volatility, J. Am. Ceramic Soc. 97 (6) (2014) 1959–1965.
[5] C. Gustavo, N.S. Jacobson, Mass spectrometric measurements of the silica activity in the Yb_2O_3–SiO_2 system and implications to assess the degradation of silicate-based coatings in combustion environments, J. Eur. Ceramic Soc. 35 (2015) 4259–4267.
[6] J. Han, Y. Wang, R. Liu, D. Jiang, Study on water vapor corrosion resistance of rare earth monosilicates RE_2SiO_5 (RE = Lu, Yb, Tm, Er, Ho,Dy, Y, and Sc) from first-principles calculations, 4, Elsevier, 2018.
[7] Z. Tian, L. Zheng, J. Wang, P. Wan, J. Li, J. Wang, Theoretical and experimental determination of the major thermo-mechanical properties of RE_2SiO_5 (RE=Tb, Dy, Ho, Er, Tm, Yb, Lu, and Y) for environmental and thermal barrier coating applications, J. Eur.Ceramic Soc. 36 (1) (2016) 189–202, doi:10.1016/j.jeurceramsoc.2015.09.013.
[8] B. Abeles, Lattice thermal conductivity of disordered semiconductor alloys at high temperatures, Phys. Rev. 131 (5) (1963) 1906–1911, doi:10.1103/PhysRev.131.1906.
[9] A. Giri, J. Braun, C. Rost, P. Hopkins, On the minimum limit to thermal conductivity of multi-atom component crystalline solid solutions based on impurity mass scattering, Scripta Materialia (138) (2017) 134–138, doi:10.1016/j.scriptamat.2017.05.045.
[10] ASTM International. Standard Test Methods for Density of Compacted or Sintered Powder Metallurgy (PM). 2020 n.d.
[11] Y. He, Rapid thermal conductivity measurement with a hot disk sensor: Part 1. Theoretical considerations, Thermochimica Acta 436 (1) (2005) 122–129, doi:10.1016/j.tca.2005.06.026.
[12] S.E. Gustafsson, Transient plane source techniques for thermal conductivity and thermal diffusivity measurements of solid materials, Rev. Sci. Instrum. 62 (3) (1991) 797–804, doi:10.1063/1.1142087.
[13] S. Malinarič, Uncertainty analysis of thermophysical property measurements of solids using dynamic methods, Int. J. Thermophys. 28 (1) (2007) 20–32, doi:10.1007/s10765-006-0134-2.
[14] D.G. Cahill, Thermal conductivity measurement from 30 to 750 K: the 3ω method, Rev. Sci. Inst. 61 (2) (1990) 802–808 10.1063/1.1141498.
[15] K. Liddell, D.P. Thompson, X-ray diffraction data for yttrium silicates, Trans. J. Br. Ceram. Soc. 85 (1) (1986) 17–22.
[16] K.A. Denault, J. Brgoch, S.D. Kloss, et al., Average and local structure, Debye temperature, and structural rigidity in some oxide compounds related to phosphor hosts, ACS Appl. Mater. Interfaces 7 (13) (2015) 7264–7272.
[17] L. León-Reina, J.M. Porras-Vázquez, E.R. Losilla, L. Moreno-Real, M.A. Aranda, Structure and oxide anion conductivity in Ln_2 (TO_4) O (Ln= La, Nd; T= Ge, Si), J. Solid State Chem. 181 (9) (2008) 2501–2506.
[18] Gentner E. Mineral-Petro Institut, Univ Heidelberg, Heidelberg, West Germany, ICDD Grant-in-Aid. 1989.
[19] R.W. Olesinski, G.J. Abbaschian, The C–Si (Carbon-Silicon) System, Bull. Alloy Phase Diagrams (5) (1984) 486–489.
[20] M.W. Hull, Accuracy, precision, and confidence in X-ray fluorescence for positive material identification, The NDT Technician 16 (1) (2017) 1–6.
[21] Zhu D, Kang L. Thermal expansion and thermal conductivity of rare earth silicates. 2006.
[22] K.N. Lee, D.S. Fox, N.P. Bansal, Rare earth silicate environmental barrier coatings for SiC/SiC composites and Si_3N_4 ceramics, J. Eur. Ceramic Soc. 25 (10) (2005) 1705–1715, doi:10.1016/j.jeurceramsoc.2004.12.013.
[23] N. Al Nasiri, N. Patra, D. Horlait, D.D. Jayaseelan, W.E. Lee, Thermal properties of rare-earth monosilicates for EBC on Si-based ceramic composites, J. Am. Ceram. Soc. 99 (2) (2016) 589–596, doi:10.1111/jace.13982.
[24] K. Fukuda, H. Matsubara, Anisotropic thermal expansion in yttrium silicate, J. Mater. Res. 18 (07) (2003) 1715–1722, doi:10.1557/JMR.2003.0236.
[25] Z.S. Khan, B. Zou, W. Huang, et al., Synthesis and characterization of Yb and Er based monosilicate powders and durability of plasma sprayed Yb_2SiO_5 coatings on C/C–SiC composites, Mater. Sci. Eng.: B 177 (2) (2012) 184–189, doi:10.1016/j.mseb.2011.12.004.

[26] M-H. Lu, H-M. Xiang, Z-H. Feng, X-Y. Wang, Y-C. Zhou, Mechanical and Thermal Properties of Yb_2 SiO_5 : A Promising Material for T/EBCs Applications, J. Am. Ceramic Soc. 99 (4) (2016) 1404–1411, doi:10.1111/jace.14085.
[27] C-W. Nan, R. Birringer, D.R. Clarke, H. Gleiter, Effective thermal conductivity of particulate composites with interfacial thermal resistance, J. Appl. Phys. 81 (10) (1997) 6692–6699, doi:10.1063/1.365209.
[28] Z. Sun, M. Li, Y. Zhou, Thermal properties of single-phase Y_2SiO_5, J. Eur. Ceram. Soc. 29 (4) (2009) 551–557, doi:10.1016/j.jeurceramsoc.2008.07.026.
[29] Al N. Nasrin, P. Niranjan, H. Denis, J.D. Doni, E. Lee William, J. Smialek, Thermal properties of rare-earth monosilicates for EBC on Si-based ceramic composites, J. Am. Ceram. Soc. 99 (2) (2015) 589–596, doi:10.1111/jace.13982.
[30] X. Ren, Z. Tian, J. Zhang, J. Wang, Equiatomic quaternary $(Y1/4Ho1/4Er1/4Yb1/4)_2SiO_5$ silicate: a perspective multifunctional thermal and environmental barrier coating material, Scripta Materialia 168 (2019) 47–50, doi:10.1016/j.scriptamat.2019.04.018.
[31] J. Gild, M. Samiee, J.L. Braun, et al., High-entropy fluorite oxides, J. Eur. Ceram. Soc. 38 (10) (2018) 3578–3584, doi:10.1016/j.jeurceramsoc.2018.04.010.
[32] J.L. Braun, C.M. Rost, M. Lim, et al., Charge-induced disorder controls the thermal conductivity of entropy-stabilized oxides, Adv. Mater. 30 (51) (2018) 1805004, doi:10.1002/adma.201805004.
[33] J. Gild, J.L. Braun, et al., A high-entropy silicide: $(Mo_{0.2}Nb_{0.2}Ta_{0.2}Ti_{0.2}W_{0.2})Si_2$, J. Materiom. 5 (3) (2020) 337–343, doi:10.1016/j.jmat.2019.03.002.
[34] Y. Ogura, Y_2SiO_5 as Oxidation Resistant Coating for C/C Composites, in: Proceedings of the 10th Whistler, Canada, 1995, pp. 767–774.
[35] S. Ramasamy, S.N. Tewari, K.N. Lee, R.T. Bhatt, D.S. Fox, EBC development for hot-pressed Y_2O_3/Al_2O_3 doped silicon nitride ceramics, Mater. Sci. Eng.: A 527 (21–22) (2010) 5492–5498, doi:10.1016/j.msea.2010.05.067.
[36] W. Hu, H. Nian, Phase evolution of reactive sputtering synthesized holmium silicate coatings, J. Am. Ceram. Soc. (102) (2018), doi:10.1111/jace.15930.
[37] Y. Dong, K. Ren, Y. Lu, Q. Wang, J. Liu, Y. Wang, High-entropy environmental barrier coating for the ceramic matrix composites, J. Eur. Ceram. Soc. 39 (7) (2019) 2574–2579, doi:10.1016/j.jeurceramsoc.2019.02.022.
[38] J. Felsche, The crystal chemistry of the rare earth silicates, Rare Earths, Springer, Berlin, Heidelberg, 1973.
[39] A.J. Fernández-Carrión, M. Allix, A.I. Becerro, Thermal expansion of rare-earth pyrosilicates, J. Am. Ceram. Soc. 96 (7) (2013) 2298–2305, doi:10.1111/jace.12388.